A&A 460, 893–899 (2006)
DOI: 10.1051/0004-6361:20065313

Astronomy & Astrophysics

On the period ratio $P_1/2P_2$ in the oscillations of coronal loops⋆

M. P. McEwan, G. R. Donnelly, A. J. Díaz, and B. Roberts

School of Mathematics and Statistics, University of St Andrews, St Andrews, Fife KY169SS, Scotland
e-mail: mike@mcs.st-and.ac.uk

Received 29 March 2006 / Accepted 11 September 2006

ABSTRACT

Aims. With strong evidence of fast and slow magnetoacoustic modes arising in the solar atmosphere there is scope for improved determinations of coronal parameters through coronal seismology. Of particular interest is the ratio $P_1/2P_2$ between the period P_1 of the fundamental mode and the period P_2 of its first harmonic; in an homogeneous medium this ratio is one, but in a more complex configuration it is shifted to lower values.
Methods. We consider analytically the effects on the different magnetohydrodynamic modes of structuring and stratification, pointing out that transverse or longitudinal structuring or gravitational stratification modifies the ratio $P_1/2P_2$.
Results. The deviations caused by gravity and structure are studied for the fast and slow modes. Structure along the loop is found to be the dominant effect.
Conclusions. The departure of $P_1/2P_2$ from unity can be used as a seismological tool in the corona. We apply our technique to the observations by Verwichte et al. (2004), deducing the density scale height in a coronal loop.

Key words. Sun: oscillations – Sun: magnetic fields – Sun: corona

1. Introduction

With the advent of space missions Solar and Heliospheric Observatory (SOHO) and the Transition Region And Coronal Explorer (TRACE) there is convincing evidence of slow and fast magnetoacoustic waves in the corona. There is observational evidence of slow modes occurring as propagating waves (DeForest & Gurman 1998; Robbrecht et al. 2001; Ofman et al. 1997, 1999; De Moortel et al. 2000, 2002a,b; King et al. 2003; Sakurai et al. 2002; McEwan & De Moortel 2006) and also as standing waves (Ofman & Wang 2002; Wang et al. 2002, 2003a,b). Fast kink waves have also been reported as standing modes (Aschwanden et al. 1999; Aschwanden et al. 2002; Nakariakov et al. 1999; Wang & Solanki 2004; Verwichte et al. 2004) but may arise also as propagating waves (Verwichte et al. 2005). Williams et al. (2002) found evidence for impulsively generated propagating fast waves. Fast sausage modes have also been identified (Nakariakov et al. 2003; Nakariakov et al. 2005; Melnikov et al. 2005). Extensive reviews of these observations and their theoretical interpretation are provided in Roberts (2000, 2004), Wang (2004), Roberts & Nakariakov (2003), Aschwanden (2004), Nakariakov & Verwichte (2005), De Moortel (2006) and Goossens et al. (2006). Waves can be utilised to provide a coronal seismology (Roberts et al. 1984; Roberts 1986, 2000, 2004, 2006; Nakariakov et al. 1999; Nakariakov & Ofman 2001), giving us indirect determinations of various coronal parameters.

The fundamental period P_1 of a MHD mode contains information mainly about the average profile of the propagation speed of the mode. Andries et al. (2005a) argued that the frequencies and damping times of a stratified loop are very close to those of an unstratified loop with the same weighted mean density, the weight depending upon the spatial structure of the mode under consideration (see also Díaz et al. 2006).

Observations of standing waves have so far mainly identified the fundamental harmonics of a vibrating loop, with evidence for higher harmonics being rare. However, Verwichte et al. (2004) have identified the fundamental and its first harmonic of the standing transverse kink mode in two cases.

Andries et al. (2005a,b) and Goossens et al. (2006) have pointed out that the identification of harmonics could provide important diagnostic information for the coronal seismology of a loop. In particular, Andries et al. (2005b) studied the ratio P_1/P_2 of the fundamental oscillation period, P_1, and its first harmonic or overtone, P_2, of a kink mode oscillation, showing that this ratio falls below 2. For standing waves on an elastic string, $P_1/P_2 = 2$ and so $P_1/2P_2 = 1$. In Andries et al. (2005b) the departure of P_1/P_2 from 2 is a consequence of the density structure along the loop, and they explore this aspect through numerical modeling of the oscillations. Their work allows a comparison between the model and the observational results of Verwichte et al. (2004), which gave $P_1/P_2 = 1.81$ in one case and $P_1/P_2 = 1.64$ in another case. Andries et al. (2005b) included density structure but ignored the effects of gravity.

We take up the suggestion that $P_1/2P_2$ may depart from unity and we argue that such a departure is a natural consequence of the structure and stratification of the medium. We study how the ratio $P_1/2P_2$ deviates from unity for fast and slow MHD modes in response to such effects as structuring in the longitudinal or transversal directions or gravity. Our main conclusion is that longitudinal structuring is the most important effect and this can be used in coronal seismology to estimate properties such as the density stratification scale.

⋆ Appendix A is only available in electronic form at http://www.aanda.org

2. Ratio of $P_1/2P_2$ for fast modes

A convenient starting point for our analysis of fast waves is the set of linearised ideal MHD equations for a straight uniform magnetic field $\boldsymbol{B}_0 = B_0\hat{\boldsymbol{z}}$, constant plasma pressure and an equilibrium density profile $\rho_0(z)$ that is structured along the z-axis (Roberts 1991; Díaz et al. 2002; Díaz 2004; see Appendix A for a derivation),

$$\frac{\partial p_{\rm T}}{\partial t} = \rho_0(z)c_{\rm A}^2(z)\frac{\partial v_z}{\partial z} - \rho_0(z)c_{\rm f}^2(z)\nabla\cdot\boldsymbol{v}, \tag{1}$$

$$\rho_0(z)\left(\frac{\partial^2}{\partial t^2} - c_{\rm A}^2(z)\frac{\partial^2}{\partial z^2}\right)\boldsymbol{v}_\perp + \nabla_\perp\frac{\partial p_{\rm T}}{\partial t} = 0, \tag{2}$$

$$\rho_0(z)\left(\frac{\partial^2}{\partial t^2} - c_{\rm T}^2(z)\frac{\partial^2}{\partial z^2}\right)v_z + \frac{c_{\rm s}^2(z)}{c_{\rm f}^2(z)}\frac{\partial}{\partial z}\left(\frac{\partial p_{\rm T}}{\partial t}\right) = 0, \tag{3}$$

where $c_{\rm s}(z) = \sqrt{\gamma p_0/\rho_0(z)}$ is the sound speed, $c_{\rm A}(z) = B_0/\sqrt{\mu\rho_0(z)}$ the Alfvén speed, and $c_{\rm f}$ and $c_{\rm T}$ are defined through $c_{\rm f}^2 = c_{\rm s}^2 + c_{\rm A}^2$ and $c_{\rm T}^{-2} = c_{\rm s}^{-2} + c_{\rm A}^{-2}$. Notice that the characteristic speeds depend on the coordinate z along the loop via the equilibrium density profile. Here $\boldsymbol{v} = \boldsymbol{v}_\perp + v_z\hat{\boldsymbol{z}}$ is the perturbation flow and p_T is the associated total (plasma plus magnetic) pressure perturbation. The effects of gravity are not included in this analysis.

Equations (1)–(3) are valid in the internal and external region separately. We use boundary conditions of continuous total pressure and velocity across the interface to model the radial dependence. In Roberts (1991) neither a uniform magnetic field nor uniform pressure was assumed but the density ρ_0 was taken to be independent of z.

Equations (1)–(3) may be used to obtain the modes of oscillation of an unbounded homogeneous cylindrical magnetic flux tube of radius a with constant densities $\rho_{\rm i}$ and $\rho_{\rm e}$ inside and outside the tube. For waves of frequency ω and longitudinal wavenumber k, the modes of oscillation of a magnetic flux tube embedded in a magnetised plasma have been discussed by Edwin & Roberts (1983), who obtained a dispersion diagram for the modes. Figure 1 displays such a diagram, obtained here for a flux tube with internal Alfvén speed $c_{\rm Ai}$ embedded in an environment with Alfvén speed $c_{\rm Ae} = 2c_{\rm Ai}$; the sound speed $c_{\rm i}$ inside the tube is $c_{\rm i} = 0.2c_{\rm Ai}$ and the sound speed $c_{\rm e}$ in the environment is $c_{\rm e} = 0.1c_{\rm Ai}$.

2.1. Magnetic structuring

The ratio $P_1/2P_2$ departs from unity even in the case of a straight homogeneous loop. To see this, consider the fast kink mode which in Fig. 1 has a phase speed $c_{\rm ph}$ $(= \omega/k)$ which in the limit of a thin tube ($ka \ll 1$) has speed c_k, where

$$c_k = \left(\frac{\rho_{\rm i}c_{\rm Ai}^2 + \rho_{\rm e}c_{\rm Ae}^2}{\rho_{\rm i} + \rho_{\rm e}}\right)^{1/2} \tag{4}$$

where $\rho_{\rm i}$ and $\rho_{\rm e}$ denote the plasma densities inside and external to the loop, respectively. In a uniform magnetic field in which the tube is defined solely by a density difference, so $\rho_{\rm i} \neq \rho_{\rm e}$, then $c_k = c_{\rm Ai}\,(2\rho_{\rm i}/\,(\rho_{\rm i} + \rho_{\rm e}))^{1/2}$; for a high density loop with $\rho_{\rm i} \gg \rho_{\rm e}$, this gives a speed $c_k = \sqrt{2}c_{\rm Ai}$, which is 41% larger than the tube's Alfvén speed $c_{\rm Ai}$.

Consider then the ratio $P_1/2P_2$ of the fundamental fast kink oscillation of period P_1 to its first harmonic of period P_2. Since $c_{\rm ph} = \omega/k$, we have an associated period $P = 2\pi/\omega = 2\pi/kc_{\rm ph}$.

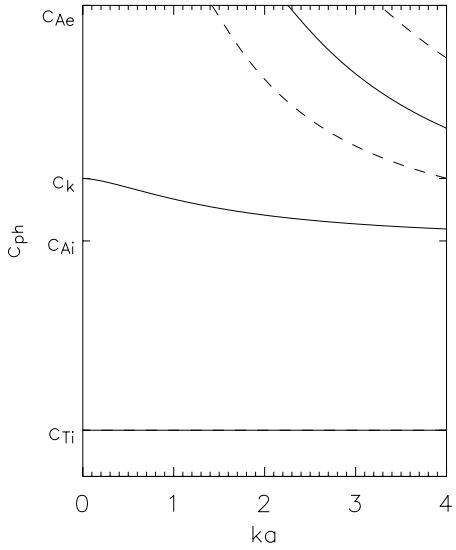

Fig. 1. The dispersion diagram for magnetoacoustic waves in a magnetic flux tube of radius a. The diagram gives the phase speed $c_{\rm ph}(=\omega/k)$ of the modes as a function of longitudinal wavenumber k (in dimensionless units of ka). The solid curves give the fast kink modes, the dashed curves are the fast sausage modes. Also shown is the weakly dispersive band of slow waves (sausage and kink) with speed close to c_{Ti}, the slow mode speed in the tube interior. Here the internal Alfvén speed $c_{\rm Ai}$ is half the Alfvén speed $c_{\rm Ae}$ in the environment, $c_{\rm i} = 0.2c_{\rm Ai}$ and $c_{\rm e} = 0.1c_{\rm Ai}$. (After Edwin & Roberts 1983).

Consider a line-tied coronal loop of length $2L$. Line-tying determines the values of the longitudinal wavenumber k that allow the oscillation to fit within the loop, so that (see Roberts et al. 1984) $k = k_n = n\pi/(2L)$, for integer n. Then we obtain a period $P = P_n$ given by

$$P_n = \frac{4L}{nc_{\rm ph}(k_n)}\cdot \tag{5}$$

The speed $c_{\rm ph}(k_n)$ varies with k_n, as shown in Fig. 1; the modes are dispersive. When $n = 1$ we obtain the fundamental mode (with $k_1 = \pi/2L$) and $n = 2$ gives its first harmonic (or overtone), with $k_2 = 2k_1 = \pi/L$). Thus

$$\frac{P_1}{2P_2} = \frac{c_{\rm ph}(k_2)}{c_{\rm ph}(k_1)}\cdot \tag{6}$$

In a medium for which dispersion is absent, $c_{\rm ph}(k_1) = c_{\rm ph}(k_2)$ and so $P_1/2P_2 = 1$. This is the situation with a sound wave or a wave on an elastic string. But here dispersion – introduced as a consequence of structuring across the magnetic field – causes this ratio to depart from unity. In fact, for the kink mode of Fig. 1, dispersion results in $c_{\rm ph}(k_1) > c_{\rm ph}(k_2)$ and so $P_1/2P_2$ is less than unity. Figure 2 displays $P_1/2P_2$ as a function of a/L, determined from Fig. 1 for a uniform tube in a uniform environment (with the density $\rho_{\rm i}$ in the loop interior exceeding the density $\rho_{\rm e}$ in the environment). The departure of $P_1/2P_2$ from unity, here a measure of the density structuring across the field, varies with loop length. For very short ($L \ll a$) or very long ($L \gg a$) loops, the ratio is close to one, but it possesses a minimum when $L \simeq a$. In coronal applications, only the results for long loops ($L \gg a$) are likely to be relevant. (In the case of fast sausage modes (shown dashed in Fig. 1), the presence of cutoff complicates the consideration of $P_1/2P_2$, since it may be that the wave is leaky.)

We can understand more fully the departure of $P_1/2P_2$ from unity in the kink mode if we focus on a thin tube ($ka \ll 1$) with

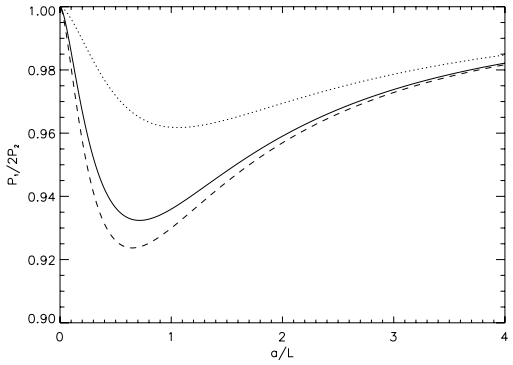

Fig. 2. $P_1/2P_2$ for the kink mode in a uniform coronal loop in a uniform environment. The dotted curve is for the case $\rho_i/\rho_e = 2$, the solid curve is for $\rho_i/\rho_e = 25/4$, and the dashed curve represents $\rho_i/\rho_e = 15$. Departures of $P_1/2P_2$ from unity are here a consequence of radial structuring ($\rho_i \neq \rho_e, c_{Ai} \neq c_{Ae}$).

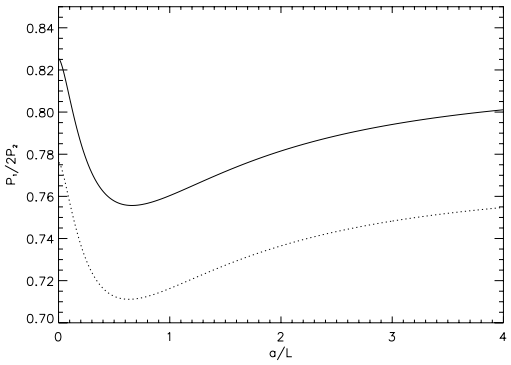

Fig. 3. $P_1/2P_2$ as a consequence of combined longitudinal and transverse structuring. The density is exponentially structured along the loop. The solid line has a base density that is 8 times the density at the apex $\left(\rho_{base}/\rho_{apex} = 8\right)$ and the dotted line has $\rho_{base}/\rho_{apex} = 16$. The tube is also structured radially with $c_{Ae}(0) = \frac{5}{2}c_{Ai}(0)$, corresponding to a tube density enhancement at the apex of $25/4$ times the environment density there.

zero plasma β. With $\beta = 0$ (sound speeds are set to zero), the kink mode in a thin tube has a phase speed c_{ph} given by (Edwin & Roberts 1983)

$$c_{ph} = c_k\left(1 - A\,(\kappa ka)^2\,K_0\,(\kappa ka)\right), \qquad ka \ll 1, \tag{7}$$

where K_0 denotes the modified Bessel function and

$$A = \frac{1}{4}\left(\frac{\rho_i - \rho_e}{\rho_i + \rho_e}\right), \qquad \kappa = \left(\frac{\rho_i - \rho_e}{\rho_i + \rho_e}\right)^{1/2}. \tag{8}$$

This relation applies strictly for $ka \ll 1$, but it is illuminating to consider its use in (6). Then

$$\frac{P_1}{2P_2} = \frac{1 - 4Ax^2K_0\,(2x)}{1 - Ax^2K_0\,(x)}, \tag{9}$$

where we have written $x = \kappa k_1 a = (\kappa\pi/2)(a/L)$. So $P_1/2P_2$ varies as a function of a/L (see Fig. 2). Expanding the denominator for small x, we obtain

$$\frac{P_1}{2P_2} \approx 1 - Ax^2\left[4K_0\,(2x) - K_0\,(x)\right]. \tag{10}$$

It is easy to show that $P_1/2P_2$ has a minimum when $x = x_m$, i.e., when $\kappa k_1 a = x_m$ so $a/L = (2/\kappa\pi)\,x_m$, with x_m being determined by the transcendental equation

$$8K_0\,(2x_m) - 2K_0\,(x_m) = 8x_mK_1\,(2x_m) - x_mK_1\,(x_m). \tag{11}$$

The corresponding minimum value of $P_1/2P_2$ is given by

$$\left(\frac{P_1}{2P_2}\right)_{min} = 1 - \frac{1}{4}\left(\frac{\rho_i - \rho_e}{\rho_i + \rho_e}\right)B_m, \tag{12}$$

where B_m depends only on x_m. Specifically, numerical determination gives $x_m = 0.48$ and $B_m = 0.19$. The important point here is to note that the shift in $P_1/2P_2$ from unity depends entirely on ρ_i and ρ_e, reaching a maximum value of $\frac{1}{4}B_m = 0.0475$ in the extreme $\rho_i \gg \rho_e$. Thus dispersion in a thin coronal flux tube produces, for the kink mode, a shift in $P_1/2P_2$ of at most 4.75%, with a corresponding minimum value of $P_1/2P_2 = 0.9525$. Actual shifts, when the full dispersion relation is used rather than the approximation, given by Eq. (7), amount to somewhat more than 4.75% (see Fig. 2), but nonetheless this provides us with a good guide as to the magnitude of the harmonic shift due to dispersion induced by structuring *across* the field.

2.2. Longitudinal structuring

We now consider the role of structuring along the magnetic field. This is the effect discussed by Andries et al. (2005b) for a different equilibrium profile. Consider again a zero-β plasma, taking an exponential density profile $\rho_i(z) = \rho_i(0)\exp(z/\Lambda_c)$ for coronal density scale height Λ_c. The density increases from a value $\rho_i(0) = \rho_{apex}$ at the loop apex ($z = 0$) to a value $\rho_i(z = L) = \rho_{base}$ at the loop base ($z = L$), which are related to the density scale height Λ_c as

$$\frac{L}{\Lambda_c} = \ln\left(\frac{\rho_{base}}{\rho_{apex}}\right). \tag{13}$$

In the zero-β limit, Eqs. (1) and (2) can be combined to obtain a single partial differential equation for the perturbed total pressure (Díaz et al. 2002; Donnelly et al. 2006),

$$\left(\frac{\partial^2}{\partial t^2} - c_A^2(z)\nabla^2\right)p_T = 0. \tag{14}$$

We follow the same procedure used in Díaz et al. (2002) to solve Eq. (14). A sum over the eigenfunctions is required to satisfy the boundary conditions at the loop surface, which leads to a system of equations for the coefficients of the eigenfunctions. The condition of having non-trivial solutions gives us the dispersion relation (see Donnelly 2006 for further details on the calculation).

The general solution is a result of a combination of two effects, radial and longitudinal structuring. Two typical curves for various ratios ρ_{base}/ρ_{apex} and $c_{Ae}(0) = 2.5c_{Ai}(0)$ are shown in Fig. 3. We highlight the fact that due to the presence of the exponential density profile the ratio $P_1/2P_2$ is now no longer equal to unity for any value of a/L. In fact, longitudinal structuring shifts the ratio even for $a/L \ll 1$ (Fig. 4). However, in addition the effect of the structuring across the loop shifts it further (though in a similar way to that shown in Fig. 2 for an unstructured loop) as a/L is increased and the dispersive nature of the mode is included. Notice in Fig. 3 that the shift due to longitudinal structuring is larger than that due to radial structuring, especially since for solar coronal loops $a/L \approx 0.01$. The previous case of an unstructured loop follows from Fig. 4 by taking the limit $\Lambda_c \to \infty$, so $L/\Lambda_c \to 0$.

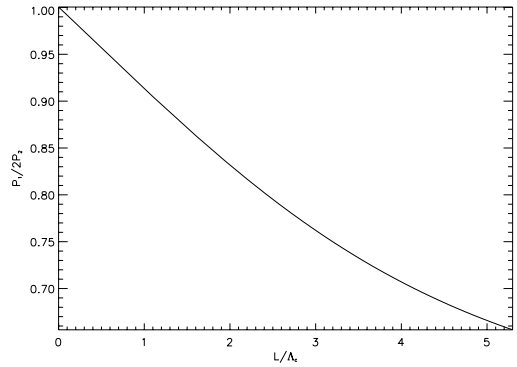

Fig. 4. $P_1/2P_2$ as a function of the inverse scale height L/Λ_c for a coronal loop of fixed length $2L$ structured exponentially in density. Here we have taken a loop of half length $L = 10^3 a$ and $c_{Ae}(0) = \frac{5}{2} c_{Ai}(0)$, so $\rho_i(0) = \frac{25}{4}\rho_e(0)$.

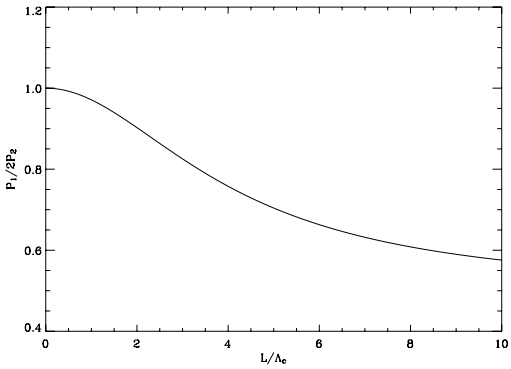

Fig. 5. $P_1/2P_2$ for a slow (or acoustic) mode in an isothermal coronal loop as a function of loop half-length L in units of the pressure scale height Λ_c. The ratio $P_1/2P_2$ is given by Eq. (24).

3. Ratio of $P_1/2P_2$ for slow modes: the Klein-Gordon equation

The Klein-Gordon equation arises in a variety of wave studies (Roberts 2004): it describes the slow mode in a loop and its reduction to a one dimensional sound wave in the low β limit of a rigid magnetic field (Roberts 2006). It also describes both sausage and kink modes in a thin photospheric flux tube in which gravitational stratification is allowed for (Rae & Roberts 1982; Spruit & Roberts 1983). The Klein-Gordon equation may be written in the form

$$\frac{\partial^2 Q}{\partial t^2} - c^2(z)\frac{\partial^2 Q}{\partial z^2} + \Omega^2(z) Q = 0, \tag{15}$$

where $Q(z,t)$ is related to the vertical motion v_z by

$$v_z(z,t) = \left(\frac{\rho_0(0)\, c^2(0)}{\rho_0(z)\, c^2(z)}\right)^{1/2} Q(z,t). \tag{16}$$

For a slow magnetoacoustic mode we have $c(z) = c_T(z)$, the tube speed, and for an acoustic mode we have $c(z) = c_s(z)$, the sound speed; $\Omega(z)$ is a cutoff frequency which depends upon gravitational stratification. In general these quantities are a function of distance along the propagation path (i.e. the loop). Writing $Q(z,t) = Q(z)\exp(i\omega t)$, for frequency ω, the Klein-Gordon Eq. (15) gives

$$\frac{\mathrm{d}^2 Q}{\mathrm{d}z^2} + \left(\frac{\omega^2 - \Omega^2(z)}{c^2(z)}\right) Q = 0. \tag{17}$$

3.1. Constant c and Ω

The simplest case to discuss is that of a medium for which the propagation speed c and the cutoff frequency Ω are constants. This case, for example, arises for an acoustic wave propagating vertically in an isothermal atmosphere. Then Eq. (17) has solution

$$Q(z) = A\sin(kz) + B\cos(kz), \tag{18}$$

where

$$\omega^2 = k^2 c^2 + \Omega^2. \tag{19}$$

We are interested in standing waves which have $Q = 0$ at the ends of a coronal loop. It is convenient to discuss separately modes that are symmetric and anti-symmetric about the apex of a loop. In a loop of length $2L$, straightened out so that $z = \pm L$ are the loop footpoints and $z = 0$ is the loop apex, the *even* modes are of the form

$$Q(z) = B\cos(kz) \tag{20}$$

and satisfy $\mathrm{d}Q/\mathrm{d}z = 0$ at the loop apex ($z = 0$); the perturbation Q has a maximum or minimum at the apex. At the loop footpoint $z = L$ we require $Q = 0$, so $kL = \left(n - \frac{1}{2}\right)\pi$, $n = 1, 2, 3, \ldots$, producing *even* mode frequencies $\omega = \omega_{2n-1}$, where

$$\omega_{2n-1}^2 = \Omega^2 + \frac{\left(n - \frac{1}{2}\right)^2 \pi^2 c^2}{L^2}. \tag{21}$$

The case $n = 1$ produces the fundamental frequency ω_1 of the loop as a whole; $n = 2$ produces the harmonic ω_3 of the loop as a whole, etc.

Similarly, we may consider the *odd* modes which leave the loop apex undisturbed, so $Q = 0$ at $z = 0$ and $z = L$. Then

$$Q(z) = A\sin(kz) \tag{22}$$

with $kL = n\pi$, $n = 1, 2, 3, \ldots$ The *odd* modes have frequencies $\omega = \omega_{2n}$ where

$$\omega_{2n}^2 = \Omega^2 + \frac{n^2\pi^2 c^2}{L^2}. \tag{23}$$

The first harmonic of the loop as a whole has a frequency ω_2, given by Eq. (23) with $n = 1$.

Thus the ratio of the fundamental and first harmonic frequencies, ω_2/ω_1, leads to P_1/P_2, with

$$\frac{P_1}{2P_2} = \left(\frac{1 + \frac{\Omega^2 L^2}{\pi^2 c^2}}{1 + \frac{4\Omega^2 L^2}{\pi^2 c^2}}\right)^{\frac{1}{2}} = \left(\frac{1 + \frac{1}{4\pi^2}\left(\frac{L}{\Lambda_c}\right)^2}{1 + \frac{1}{\pi^2}\left(\frac{L}{\Lambda_c}\right)^2}\right)^{1/2}, \tag{24}$$

with $\Lambda_c = c/2\Omega$. It is immediately clear that $\frac{1}{2} \le P_1/2P_2 \le 1$, becoming one when $\Omega = 0$. The case when $\Omega = 0$ corresponds to the uniform loop in a uniform environment, with no gravitational stratification.

Figure 5 displays the ratio $P_1/2P_2$ as a function of loop half-length L (measured in units of the density scale height Λ_c), as determined by Eq. (24). Stratification of density causes $P_1/2P_2$ to fall off from unity, with the effect being most marked in very long loops ($L \gg \Lambda_c$). In general, coronal loops have $L \simeq \Lambda_c$, and the departure of $P_1/2P_2$ from unity is only slight. In fact the magnitude of the shift of $P_1/2P_2$ due to stratification by gravity

for the slow mode for a loop of typical half length ($L \simeq \Lambda_c$) is comparable to the magnitude of the shift brought about by radial magnetic structuring for the fast mode. The slow mode is much less dispersive than the fast mode so the correction due to radial structuring is even smaller. For example, a loop with internal density $\rho_i = \frac{25}{4}\rho_e$, half-length $L = 5 \times 10^4$ km and radius $a = 5000$ km, so $a/L = 1/20$, produces a kink mode ratio of $P_1/2P_2 = 0.995$ (see Fig. 2). This may be compared with an acoustic wave in an isothermal atmosphere with sound speed $c = c_s = 200\ \mathrm{km\,s^{-1}}$ for which the acoustic cutoff frequency is $\Omega\,(= c_s/2\Lambda_c = \gamma g/2c_s)$ and $c_s/\Omega = 1.78 \times 10^5$ km, resulting in $P_1/2P_2 = 0.988$. This is a shift from unity of 0.012 or 1.2%. Typically, slow or acoustic modes produces a small harmonic shift due to gravity in all but extremely long loops.

3.2. Non-constant c and Ω

Consider Eq. (15) for the case when c and Ω vary with z. To be specific, we discuss the case of an acoustic wave propagating vertically in an atmosphere with a linear temperature profile for which the propagation speed c is the sound speed $c_s(z)$:

$$c^2 = c_s^2(z) = c_{\mathrm{apex}}^2\,(1 - \alpha z)\,. \tag{25}$$

The sound speed squared c_s^2 decreases (for $\alpha > 0$) linearly with distance z from the loop apex. Suppose that the loop sound speed decreases from a value c_{apex} at the loop apex ($z = 0$) to c_{base} at the loop base $z = L$. Then

$$\alpha = \frac{\lambda^2 - 1}{\lambda^2 L}, \qquad \lambda = \frac{c_{\mathrm{apex}}}{c_{\mathrm{base}}}\cdot \tag{26}$$

The pressure scale height is $\Lambda_c(z) = \Lambda_c\,(0)\,(1 - \alpha z)$, and the cut-off frequency is given by (see Lamb 1932; Roberts 2004)

$$\Omega^2(z) = \frac{c_s^2}{4\Lambda_c^2}\left(1 - 2\Lambda_c^{'}\right) = \left(\frac{(\gamma g)^2}{4c_{\mathrm{apex}}^2} + \frac{\gamma\alpha g}{2}\right)\frac{1}{(1 - \alpha z)}, \tag{27}$$

where a dash ($'$) denotes the derivative with respect to z. Writing $u = (1 - \alpha z)$, Eq. (17) becomes

$$\frac{\mathrm{d}^2 Q}{\mathrm{d}u^2} + \left(\frac{\omega^2}{\alpha^2 c_{\mathrm{apex}}^2}\frac{1}{u} - \frac{M_0}{\alpha^2 c_{\mathrm{apex}}^2}\frac{1}{u^2}\right)Q = 0, \tag{28}$$

where

$$M_0 = \frac{\gamma^2 g^2}{4c_{\mathrm{apex}}^2} + \frac{\gamma g \alpha}{2}\cdot \tag{29}$$

The substitutions $Q = sY\,(s)$ and $s = u^{1/2}$, with $x = \beta_0 s$ and $\beta_0^2 = \frac{4\omega^2}{\alpha^2 c_{\mathrm{apex}}^2}$, transform Eq. (28) into Bessel's equation (Abramowitz & Stegun 1964)

$$\frac{\mathrm{d}^2 Y}{\mathrm{d}x^2} + \frac{1}{x}\frac{\mathrm{d}Y}{\mathrm{d}x} + \left(1 - \frac{\nu^2}{x^2}\right)Y = 0. \tag{30}$$

Accordingly, the solution to Eq. (28) is (James 2003)

$$Q(z) = (1 - \alpha z)^{\frac{1}{2}}\left[AJ_\nu\left(\frac{2\omega}{\alpha c_{\mathrm{apex}}}(1 - \alpha z)^{\frac{1}{2}}\right) + BY_\nu\left(\frac{2\omega}{\alpha c_{\mathrm{apex}}}(1 - \alpha z)^{\frac{1}{2}}\right)\right], \tag{31}$$

where

$$\nu = 1 + \frac{\gamma g}{\alpha c_{\mathrm{apex}}^2}\cdot \tag{32}$$

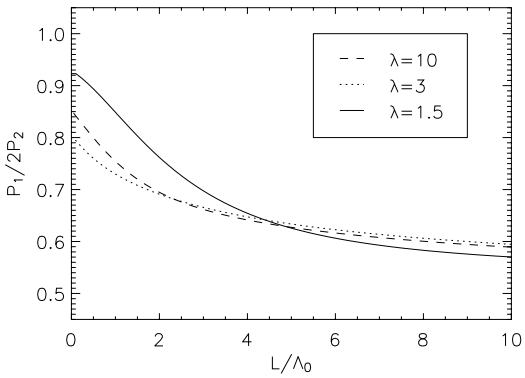

Fig. 6. The ratio $P_1/2P_2$ for a sound wave in a non-isothermal loop of length $2L$. The sound speed squared varies linearly with distance, falling from a value c_{apex} at the loop apex to $c_{\mathrm{base}}\left(=c_{\mathrm{apex}}/\lambda\right)$ at its base. When λ is close to unity we recover the isothermal case (cf. Fig. 5).

Consider the *odd* modes, satisfying $Q = 0$ at the loop apex $z = 0$ and at the loop base $z = L$. Then

$$J_\nu(x)\,Y_\nu(\lambda x) - J_\nu(\lambda x)\,Y_\nu(x) = 0, \tag{33}$$

where the arguments of the Bessel functions are:

$$x = \frac{2\omega}{\alpha c_{\mathrm{apex}}}\frac{c_{\mathrm{base}}}{c_{\mathrm{apex}}}, \qquad \lambda = \frac{c_{\mathrm{apex}}}{c_{\mathrm{base}}}\cdot \tag{34}$$

This is the dispersion relation for the odd acoustic modes in a gravitationally stratified atmosphere of a non-isothermal loop.

In a similar way, we can obtain the dispersion relation for the *even* modes which satisfy $Q = 0$ at $z = L$ and have $\mathrm{d}Q/\mathrm{d}z = 0$ at $z = 0$:

$$J_\nu(x)\,Y_\nu(\lambda x) - J_\nu(\lambda x)\,Y_\nu(x) + (\lambda x)\left(J_\nu(x)\,Y_\nu^{'}(\lambda x) - J_\nu^{'}(\lambda x)\,Y_\nu(x)\right) = 0. \tag{35}$$

Here a dash denotes the derivative of a Bessel function: $J_\nu^{'}(z) = \mathrm{d}J_\nu(z)/\mathrm{d}z$, etc.

Equations (33) and (35) determine the dimensionless frequency $2\omega/\alpha c_{\mathrm{apex}}$ for various values of $c_{\mathrm{base}}/c_{\mathrm{apex}}$ and ν. The actual frequency ω is determined once the base sound speed c_{base} and the temperature gradient are specified. It is interesting to note that the structure of Eqs. (33) and (35) remains even in the absence of gravity ($g = 0$), though the order ν of the Bessel functions then reduces to unity. Thus a shift in the ratio of $P_1/2P_2$ occurs as a consequence of non-isothermality, even if gravity is ignored. Equations (33) and (35) are solved numerically for various values of $\lambda = c_{\mathrm{apex}}/c_{\mathrm{base}}$, the ratio of the sound speed c_{apex} at the loop apex to the sound speed c_{base} at its base. Equation (35) provides the period P_1 and its first harmonic gives P_2 and is determined by Eq. (33). The ratio $P_1/2P_2$ is displayed in Fig. 6. When λ is close to unity, the loop is almost isothermal and $P_1/2P_2$ is close to unity (though decreasing with increasing loop length). But for a more strongly structured sound speed, the shift from unity in $P_1/2P_2$ is stronger. For example, for a base sound speed of $c_{\mathrm{base}} = 100\ \mathrm{km\,s^{-1}}$ and an apex sound speed of $c_{\mathrm{apex}} = 150\ \mathrm{km\,s^{-1}}$, so $\lambda = 1.5$, Fig. 6 shows that $P_1/2P_2 \simeq 0.92$ in short loops ($L \ll \Lambda_c$) and falling to approximately 0.58 in extremely long loops ($L \simeq 10\Lambda_c$). For loops with a larger temperature gradient ($\lambda \gg 1$), the immediate deviation of $P_1/2P_2$ from unity becomes more significant for short loops; however, for long loops the behaviour of $P_1/2P_2$ is similar to the isothermal case.

3.3. Isobaric loop without gravity

We have seen in the above that structuring along the loop introduces a shift in $P_1/2P_2$, even in the absence of gravity (which reduces the cutoff frequency Ω to zero). Accordingly, consider Eq. (15) in the absence of a cutoff frequency, $\Omega = 0$:

$$\frac{\partial^2 Q}{\partial t^2} - c^2(z)\frac{\partial^2 Q}{\partial z^2} = 0. \tag{36}$$

This equation can also be deduced from Eqs. (1)–(3) by assuming $L \gg a$ and using then a stretching coordinate in the radial direction (see Roberts 2006). The propagation speed in Eq. (36) can be the sound speed $c = c_s$ for a sound wave or the tube speed $c = c_T$ for a slow mode. In either case, we see that $c^2(z)$ is of the form $c^2(z) = c^2(0)\rho_0(0)/\rho_0(z)$. Consider, then, the slow mode, with $c = c_T$, and suppose that the density $\rho_0(z)$ increases exponentially in chromospheric footpoint layers but is otherwise uniform; thus

$$c_T^2(z) = \begin{cases} c_T^2(0), & 0 \le |z| \le W, \\ c_T^2(0)\mathrm{e}^{(-(|z|-W))/\Lambda_c}, & W \le |z| \le L. \end{cases} \tag{37}$$

The variation in propagation speed $c_T(z)$ is confined to footpoint layers of width $(L - W)$; the scale of variation is determined by Λ_c, which is related to the density ρ_{base} in the footpoints and the density ρ_{apex} at the loop apex through

$$\Lambda_c = (L - W) \,/\, \ln\left(\rho_{base}/\rho_{apex}\right). \tag{38}$$

Equation (36) may be solved for the profile in Eq. (37), with the result that even modes satisfy the dispersion relation (see Díaz & Roberts 2006):

$$\tan\frac{\omega W}{c_{T0}} = \frac{J_1[D(\omega)]Y_0[E(\omega)] - Y_1[D(\omega)]J_0[E(\omega)]}{J_0[D(\omega)]Y_0[E(\omega)] - Y_0[D(\omega)]J_0[E(\omega)]}, \tag{39}$$

where the arguments of the Bessel functions are:

$$D(\omega) = \frac{\omega}{c_T(0)}2\Lambda_c, \qquad E(\omega) = \frac{\omega}{c_T(0)}2\Lambda_c\mathrm{e}^{(L-W)/(2\Lambda_c)}. \tag{40}$$

In fact, Eq. (39) reduces to Eq. (35) in the limit $W = 0$, as may be seen as follows. In Sect. 3.2 a fully stratified loop was considered, so we have $W = 0$ in Eq. (37). Therefore, the left-handside of Eq. (39) vanishes, implying that

$$J_1[D(\omega)]Y_0[E(\omega)] - Y_1[D(\omega)]J_0[E(\omega)] = 0. \tag{41}$$

Also, in the absence of gravity Eq. (32) gives $\nu = 1$. By writing $x = D(\omega)$ and using the recurrence relation of Bessel functions, $Z_1(z) + zZ_1'(z) = zZ_0(z)$, with Z the Bessel function J or Y, we recover Eq. (35).

We may determine $P_1/2P_2$ using dispersion relation Eq. (39) and a similar relation for the odd modes. The results are displayed in Fig. 7. Notice that for small W/L (e.g. $W/L = 0.1$), for which the exponential variation covers most of the loop, we obtain results similar to Fig. 4, as the density profile for each case is similar. However, a direct comparison with Fig. 4 is not possible as it refers to the kink mode whereas here we consider the slow mode. On the other hand, for a thin chromospheric layer (for which W is comparable to L), $P_1/2P_2$ returns to unity unless the base density is very high.

Finally, comparing these results with those of the Klein-Gordon equation we can see that the longitudinal structure alone reproduces the profiles obtained with the inclusion of gravity. For example, comparing Fig. 5 with the plot for a fully stratified loop in Fig. 7 (solid line) we see that the shape is similar, since the density ratio is related to the inverse scale length L/Λ_c by Eq. (38) with $W = 0$.

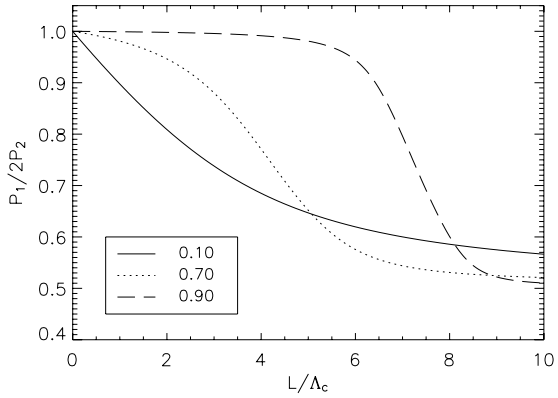

Fig. 7. $P_1/2P_2$ as a function of the inverse scale height L/Λ_c, for various chromospheric layers of dimensionless depth W/L (= 0.1, 0.7, 0.9).

4. Comparison with observational data

We have shown that some properties of the equilibrium can be obtained by studying the shift of $P_1/2P_2$ from unity. Currently, observations have indicated this effect (without interpretation) purely for the fast modes of coronal loops. We have shown in Sect. 2 that the main cause for the shift in these modes lies in the structure along the magnetic field. For an exponentially stratified loop the ratio $P_1/2P_2$ depends on the density scale height.

As an illustration, we consider the observational data in Verwichte et al. (2004) (Table II). They reported two periods in two of their time series (labelled "C" and "D") which were interpreted as the fundamental and first harmonics of the loop. The values of $P_1/2P_2$ obtained from the wavelet analysis are (Verwichte et al. 2004)

$$\left.\frac{P_1}{2P_2}\right|_C = 0.91 \pm 0.16, \qquad \left.\frac{P_1}{2P_2}\right|_D = 0.82 \pm 0.15, \tag{42}$$

in which the error bars have been calculated by the usual formulae for propagation of errors in derived magnitudes. In case C the value of the shift lies in the uncertainty range, but in case D the observations clearly point to a shift in $P_1/2P_2$. Using Fig. 4, we deduce

$$\left.\frac{L}{\Lambda_c}\right|_C = 1.0 \pm 2.2, \qquad \left.\frac{L}{\Lambda_c}\right|_D = 2.2 \pm 2.7. \tag{43}$$

Hence, using the loop lengths given in Verwichte et al. (2004), namely $2L = 218$ Mm for case C and $2L = 228$ Mm for case D, we obtain $\Lambda_c = 109 \pm 240$ Mm for case C and $\Lambda_c = 52 \pm 62$ Mm for case D. Unfortunately, in both cases the relative errors are large because of the flatness of the curves in Fig. 4, but these values nonetheless indicate the potential for what can be achieved. The equilibrium density ratio ρ_{base}/ρ_{apex} can also be obtained with Eq. (13), giving 2.8 for case C and 8.7 for case D, but the error bars are very large.

Notice that this procedure gives us a value of the ratio L/Λ_c which is independent of other considerations. This is an important advantage over other quantities deduced from coronal seismology, such as the determination of the magnetic field strength (Nakariakov & Ofman 2001), for which the values of other unknowns (e.g. the equilibrium coronal density) need to be assumed.

5. Discussion and conclusion

In this work we have explored the various effects which cause the ratio $P_1/2P_2$ to depart from unity, its value in a homogeneous

medium. Magnetic structuring, due principally to density contrast between the interior and exterior of a loop, causes fast magnetoacoustic waves to be dispersive, and this manifests itself in the ratio $P_1/2P_2$. Longitudinal structuring or stratification has a more significant effect than radial structuring, producing a larger departure from unity in $P_1/2P_2$. Longitudinal structure has also been considered by Andries et al. (2005b). We have illustrated the effect for a simple flux tube with a discrete density profile, but we can anticipate similar results for any radial structure (e.g. the Epstein profile). Of course, other effects such as magnetic flux tube expansion or non-adiabatic damping may also produce a shift in $P_1/2P_2$ from unity; however, such effects are left for a future study.

Slow magnetoacoustic waves are only very weakly dispersive, so shifts in $P_1/2P_2$ due to radial structuring are small. However, longitudinal structuring or stratification has a more important role here too, reducing $P_1/2P_2$ below unity (becoming 0.5 in the limit of an infinitely long loop). The presence of a gravitational force (as opposed to longitudinal structuring by whatever effect) complicates the behaviour of $P_1/2P_2$, but the effects are generally small in the corona (because of the high pressure scale height).

The results presented here can be used to extract information about the equilibrium state of a coronal loop. Previous work (e.g. Nakariakov & Ofman 2001) have studied the relevance for coronal seismology of the fundamental period, which allows us to deduce global properties of the loop, such as the mean density or the magnetic field strength. However, observational measurements of $P_1/2P_2$ gives information about smaller scales, and we have used this to estimate the structure's length scale for the fast mode (or the ratio between the footpoint and apex density). In principle, if all the harmonics could be observed, we could invert the problem and obtain a density profile (as it is currently done in helioseismology, where thousands of modes are reported). But with two coronal modes only currently observed we are not able to obtain such detailed information. Our method can also be applied to slow modes, but there are currently no observations of $P_1/2P_2$ for slow modes. On the other hand, it is interesting to note that more than one mode has been detected in prominences (Régnier et al. 2001; Pouget et al. 2006). Currently, only information relating to the fundamental harmonics of each prominence oscillation family is used for seismology, but similar techniques could be applied in the future for extracting information from the first (and higher) harmonics.

In conclusion, we have demonstrated how the individual contributions cause a deviation of $P_1/2P_2$ from unity, an effect highlighted in Andries et al. (2005b). Lateral structure, longitudinal structure and density stratification all play a part in forming $P_1/2P_2$, but we conclude that longitudinal structure is the key ingredient for magnetoacoustic modes.

Acknowledgements. M.P.M. and G.D. acknowledge financial support from the Particle Physics and Astronomy Research Council. A.J.D. acknowledges support from PPARC on the St Andrews Solar Theory Rolling Grant. The authors would also like to thank Erwin Verwichte, Jesse Andries and the anonymous referee for their useful comments in improving this paper.

References

Abramowitz, M., & Stegun, I. A. 1964, Handbook of Mathematical Functions, National Bureau of Standards
Andries, J., Goossens, M., Hollweg, J. V., Arregui, I., & Van Doorsselaere, T. 2005a, A&A, 430, 1109
Andries, J., Arregui, I., & Goossens, M. 2005b, ApJ, 624, L57
Aschwanden, M. J. 2004, Physics of The Solar Corona (Berlin: Springer)
Aschwanden, M. J., Fletcher, L., Schrijver, C. J., & Alexander, D. 1999, ApJ, 520, 880
Aschwanden, M. J., Brown, J. C., & Kontar, E. P. 2002, in Solar Variability: From Core to Outer Frontiers, ed. J. Kuijpers, ESA SP-506, 275
De Moortel, I. 2006, Phil. Trans. R. Soc. A, 364, 461
De Moortel, I., Ireland, J., & Walsh, R. W. 2000, A&A, 355, L23
De Moortel, I., Hood, A. W., Ireland, J., & Walsh, R. W. 2002a, in Solar Variability: From Core to Outer Frontiers, ed. J. Kuijpers, ESA SP-506, 509
De Moortel, I., Ireland, J., Walsh, R., & Hood, A. 2002b, Sol. Phys., 209, 89
DeForest, C. E., & Gurman, J. B. 1998, ApJ, 501, L217
Díaz, A. J. 2004, Fast Magnetohydrodynamic Waves in Line-tied Solar Coronal Flux Tubes, Ph.D. Thesis, Universitat de les Illes Balears
Díaz, A. J., & Roberts, B. 2006, A&A, 458, 975
Díaz, A. J., Oliver, R., & Ballester, J. L. 2002, ApJ, 580, 550
Díaz, A. J., Oliver, R., & Ballester, J. L. 2006, ApJ, 645, 766
Donnelly, G. R. 2006, Magnetohydrodynamic Oscillations in the Solar Corona, Ph.D. Thesis, University of St Andrews
Donnelly, G. R., Díaz, A. J., & Roberts, B. 2006, A&A, in press
Edwin, P. M., & Roberts, B. 1983, Sol. Phys., 88, 179
Goossens, M., Andries, J., & Arregui, I. 2006, Phil. Trans. R. Soc. A, 364, 433
James, L. 2003, Coronal Loop Oscillations, Master's thesis, School of Mathematics, University of St Andrews
King, D. B., Nakariakov, V. M., Deluca, E. E., Golub, L., & McClements, K. G. 2003, A&A, 404, L1
Lamb, H. 1932, Hydrodynamics (Cambridge University Press)
McEwan, M. P., & De Moortel, I. 2006, A&A, 448, 763
Melnikov, V. F., Reznikova, V. E., Shibasaki, K., & Nakariakov, V. M. 2005, A&A, 439, 727
Nakariakov, V. M., & Ofman, L. 2001, A&A, 372, L53
Nakariakov, V. M., & Verwichte, E. 2005, Living Rev. Sol. Phys., http://www.livingreviews.org/lrsp-2005-3
Nakariakov, V. M., Ofman, L., Deluca, E. E., Roberts, B., & Davila, J. M. 1999, Science, 285, 862
Nakariakov, V. M., Melnikov, V. F., & Reznikova, V. E. 2003, A&A, 412, L7
Nakariakov, V. M., Melnikov, V. F., & Reznikova, V. E. 2005, in ed. A. V. Stepanov, E. E. Benevolenskaya, & A. G. Kosovichev, IAU Symp., 653
Ofman, L., & Wang, T. 2002, ApJ, 580, L85
Ofman, L., Romoli, M., Poletto, G., Noci, G., & Kohl, J. L. 1997, ApJ, 491, L111
Ofman, L., Nakariakov, V. M., & DeForest, C. E. 1999, ApJ, 514, 441
Pouget, G., Bocchialini, K., & Solomon, J. 2006, A&A, 450, 1189
Rae, I. C., & Roberts, B. 1982, ApJ, 256, 761
Régnier, S., Solomon, J., & Vial, J. C. 2001, A&A, 376, 292
Robbrecht, E., Verwichte, E., Berghmans, D., et al. 2001, A&A, 370, 591
Roberts, B. 1986, in Coronal and Prominence Plasmas, 325
Roberts, B. 1991, in Advances in Solar System Magnetohydrodynamics, ed. E. R. Priest, & A. W. Hood (Cambridge University Press), 105
Roberts, B. 2000, Sol. Phys., 193, 139
Roberts, B. 2004, in SOHO 13 Waves, Oscillations and Small-Scale Transients Events in the Solar Atmosphere: Joint View from SOHO and TRACE, ESA SP-547, 1
Roberts, B. 2006, Phil. Trans. R. Soc. A, 364, 447
Roberts, B., & Nakariakov, V. M. 2003, in Turbulence, Waves and Instabilities in the Solar Plasma, 167
Roberts, B., Edwin, P. M., & Benz, A. O. 1984, ApJ, 279, 857
Sakurai, T., Ichimoto, K., Raju, K. P., & Singh, J. 2002, Sol. Phys., 209, 265
Spruit, H. C., & Roberts, B. 1983, Nature, 304, 401
Verwichte, E., Nakariakov, V. M., Ofman, L., & Deluca, E. E. 2004, Sol. Phys., 233, 77
Verwichte, E., Nakariakov, V. M., & Cooper, F. C. 2005, A&A, 430, L65
Wang, T. J. 2004, in SOHO 13 Waves, Oscillations and Small-Scale Transients Events in the Solar Atmosphere: Joint View from SOHO and TRACE, ESA SP-547, 417
Wang, T. J., & Solanki, S. K. 2004, A&A, 421, L33
Wang, T. J., Solanki, S. K., Curdt, W., Innes, D. E., & Dammasch, I. E. 2002, ApJ, 574, L101
Wang, T. J., Solanki, S. K., Curdt, W., et al. 2003a, A&A, 406, 1105
Wang, T. J., Solanki, S. K., Innes, D. E., Curdt, W., & Marsch, E. 2003b, A&A, 402, L17
Williams, D. R., Mathioudakis, M., Gallagher, P. T., et al. 2002, MNRAS, 336, 747

Online Material

Appendix A: Derivation of Eqs. (1)–(3)

We derive Eqs. (1)–(3), following Díaz (2004).

The starting point is the set of linearised ideal MHD equations for a uniform magnetic field $\boldsymbol{B}_0 = B_0\hat{\boldsymbol{z}}$, in absence of gravity and with constant plasma pressure and a density profile that is stratified along the z-axis, $\rho_0(z)$:

$$\frac{\partial \rho}{\partial t} + \rho_0(z)(\nabla\cdot\boldsymbol{v}) + (\boldsymbol{v}\cdot\nabla)\rho_0(z) = 0, \tag{A.1}$$

$$\frac{\partial \boldsymbol{B}}{\partial t} = \nabla\times(\boldsymbol{v}\times\boldsymbol{B}_0), \tag{A.2}$$

$$\rho_0(z)\frac{\partial \boldsymbol{v}}{\partial t} = -\nabla p_\mathrm{T} + \frac{1}{\mu}(\boldsymbol{B}_0\cdot\nabla)\boldsymbol{B}, \tag{A.3}$$

$$\frac{\partial p}{\partial t} + (\boldsymbol{v}\cdot\nabla)p_0 = c_\mathrm{s}^2\left(\frac{\partial\rho}{\partial t} + (\boldsymbol{v}\cdot\nabla)\rho_0(z)\right). \tag{A.4}$$

Here $\boldsymbol{B}$ denotes the perturbed magnetic field, p_T is the total pressure perturbation, $\boldsymbol{v} = \boldsymbol{v}_\perp + v_z\hat{\boldsymbol{z}}$ is the perturbation flow and ρ the perturbed density.

The induction Eq. (A.2), may be expanded to yield

$$\frac{\partial \boldsymbol{B}}{\partial t} = B_0\frac{\partial \boldsymbol{v}}{\partial z} - B_0\hat{\boldsymbol{z}}(\nabla\cdot\boldsymbol{v}), \tag{A.5}$$

in which the assumption of uniform magnetic field $\boldsymbol{B}_0$ has been used.

In the following development, the symbol $\perp$ denotes the components of the perturbed quantities and gradients perpendicular to $\boldsymbol{B}_0$. Using Eq. (A.5), the perpendicular component of Eq. (A.3) can be rewritten as

$$\rho_0\left[\frac{\partial^2}{\partial t^2} - c_\mathrm{A}^2(z)\frac{\partial^2}{\partial z^2}\right]\boldsymbol{v}_\perp + \nabla_\perp\frac{\partial p_\mathrm{T}}{\partial t} = 0, \tag{A.6}$$

where $c_\mathrm{A} = \sqrt{B_0^2/\mu\rho_0(z)}$ denotes the Alfvén speed.

Before dealing with the parallel component another expression for the perturbed total pressure is required. From Eq. (A.4) we have

$$\frac{\partial p}{\partial t} = -(\boldsymbol{v}\cdot\nabla)p_0(z) - \rho_0(z)c_\mathrm{s}^2(z)\,\nabla\cdot\boldsymbol{v}. \tag{A.7}$$

Using the definition of the magnetic pressure and Eq. (A.5) we also obtain

$$\frac{\partial p_\mathrm{m}}{\partial t} = \frac{B_0}{\mu}\frac{\partial B_z}{\partial t} = -\rho_0 c_\mathrm{A}^2(z)\,\nabla_\perp\cdot\boldsymbol{v}_\perp. \tag{A.8}$$

Equations (A.7) and (A.8) then give an expression for the perturbed total pressure, namely

$$\begin{aligned}\frac{\partial p_\mathrm{T}}{\partial t} &= \frac{\partial p}{\partial t} + \frac{\partial p_\mathrm{m}}{\partial t} = -v_z\frac{\partial p_0}{\partial z} - \rho_0(z){c_\mathrm{s}}^2(z)\frac{\partial v_z}{\partial z}\\ &-\rho_0 c_\mathrm{f}^2(z)\nabla_\perp\cdot\boldsymbol{v}_\perp = \rho_0(z)c_\mathrm{A}^2(z)\frac{\partial v_z}{\partial z} - \rho_0 c_\mathrm{f}^2(z)\nabla\cdot\boldsymbol{v},\end{aligned} \tag{A.9}$$

where $c_\mathrm{s}(z) = \sqrt{\gamma p_0/\rho_0(z)}$ is the sound speed and $c_\mathrm{f}^2 = {c_\mathrm{s}}^2 + c_\mathrm{A}^2$. In the last equality of Eq. (A.9) it has also been assumed that p_0 is constant, so its derivative along the field vanishes.

Finally, the component of Eq. (A.3) along the field gives

$$\begin{aligned}&\rho_0(z)\frac{\partial^2 v_z}{\partial t^2} + \frac{\partial}{\partial z}\frac{\partial p_\mathrm{T}}{\partial t} - \frac{B_0^2}{\mu}\frac{\partial^2 v_z}{\partial z^2} = -\frac{B_0^2}{\mu}\frac{\partial}{\partial z}(\nabla\cdot\boldsymbol{v}) =\\ &-\rho_0(z)c_\mathrm{A}^2(z)\frac{\partial}{\partial z}\left[\frac{c_\mathrm{A}^2(z)}{{c_\mathrm{f}}^2(z)}\frac{\partial v_z}{\partial z} - \frac{1}{\rho_0(z){c_\mathrm{f}}^2(z)}\frac{\partial p_\mathrm{T}}{\partial t}\right].\end{aligned} \tag{A.10}$$

Now $c_\mathrm{s}(z)$, $c_\mathrm{A}(z)$ and $c_\mathrm{f}(z)$ depend on z via the equilibrium density, the equilibrium magnetic field strength being constant. Therefore, for our equilibrium model the products

$$\rho_0(z)c_\mathrm{A}^2(z) = \frac{B_0^2}{\mu}, \quad \rho_0(z){c_\mathrm{s}}^2(z) = \gamma p_0, \quad \rho_0 c_\mathrm{f}^2(z), \ \frac{c_\mathrm{A}^2(z)}{c_\mathrm{f}^2(z)} \tag{A.11}$$

are all constants so the derivative in Eq. (A.10) only affects v_z and p_T. Thus Eq. (A.10) can be recast in the form:

$$\rho_0\left[\frac{\partial^2}{\partial t^2} - c_\mathrm{T}^2(z)\frac{\partial^2}{\partial z^2}\right]v_z + \frac{c_\mathrm{s}^2(z)}{c_\mathrm{f}^2(z)}\frac{\partial}{\partial z}\left(\frac{\partial p_\mathrm{T}}{\partial t}\right) = 0, \tag{A.12}$$

where $c_\mathrm{T}^{-2} = {c_\mathrm{s}}^{-2} + c_\mathrm{A}^{-2}$.

Equations (A.6), (A.9) and (A.10) are Eqs. (1)–(3). They are formally the same as in Roberts (1991), although in that paper the details of the derivation are slightly different: they were deduced with the assumption of Cartesian coordinates and with $B_0(x)$ and $\rho_0(x)$ instead of $\rho_0(z)$.

Since $\beta \ll 1$ in the solar corona, we can restrict ourselves to studying the oscillatory modes in the low-beta limit. This assumption implies $c_\mathrm{s} \to 0$, $c_\mathrm{T} \to 0$ and $c_\mathrm{f} \to c_\mathrm{A}$. Now, selecting the velocity components as our dependent variables leads to a pair of coupled partial differential equations, although by choosing the total pressure perturbation, p_T, as our dependent variable a single partial differential equation is obtained.

First of all, from Eq. (A.10) in the low-beta limit we have $v_z = 0$, pointing out that the slow mode is removed in this limit. Then, we take the gradient in the perpendicular plane of Eq. (A.6) and use $\nabla_\perp\rho_0(z) = 0$ and $\nabla_\perp(\rho_0(z)c_\mathrm{A}^2(z)) = 0$, giving

$$\rho_0(z)\left[\frac{\partial^2}{\partial t^2} - c_\mathrm{A}^2(z)\frac{\partial^2}{\partial z^2}\right]\nabla_\perp\cdot\boldsymbol{v}_\perp + \nabla_\perp\cdot\left(\nabla_\perp\frac{\partial p_\mathrm{T}}{\partial t}\right) = 0. \tag{A.13}$$

Next, we write Eq. (A.9) in the low-beta limit,

$$\frac{\partial p_\mathrm{T}}{\partial t} = -\rho_0 c_\mathrm{A}^2(z)\nabla_\perp\cdot\boldsymbol{v}_\perp, \tag{A.14}$$

and then we may eliminate the velocity components in Eq. (A.13), which can be cast as

$$\left[\frac{\partial^2}{\partial t^2} - c_\mathrm{A}^2(z)\frac{\partial^2}{\partial z^2}\right]\frac{\partial p_\mathrm{T}}{\partial t} - c_\mathrm{A}^2(z)\nabla_\perp\cdot\left(\nabla_\perp\frac{\partial p_\mathrm{T}}{\partial t}\right) = 0. \tag{A.15}$$

Thus, we have only one partial differential equation to solve. In any orthonormal coordinate system (such as the cylindrical and Cartesian ones) in which one of the basis vectors points in the z-direction, the operator $\nabla_\perp\cdot\nabla_\perp$ is equal to $\nabla_\perp^2$. Thus, finally, we conclude that

$$\left[\frac{\partial^2}{\partial t^2} - c_\mathrm{A}^2(z)\nabla^2\right]p_\mathrm{T} = 0, \tag{A.16}$$

which is Eq. (14).